Polymer Testing 122 (2023) 108026

Contents lists available at ScienceDirect

Polymer Testing

journal homepage: www.elsevier.com/locate/polytest

Light responsive self-healable carbon nanotube/polyurethane smart networks with precisely remote-controlled shape-changing properties

Xiaohu Chen [a,b], Yonggui Liu [a], Junfeng Li [b], Tuck-Whye Wong [c], Tao Chen [a,**], Ting Zhang [a,***], Li Wang [a,b,*]

[a] Department of Biomedical Engineering, School of Big Health and Intelligent Engineering, Chengdu Medical College, Chengdu, 610500, China
[b] College of Materials, Chemistry & Chemical Engineering, Chengdu University of Technology, Chengdu, 610059, Sichuan, PR China
[c] Advanced Membrane Technology Centre, Universiti Teknologi Malaysia, Johor, 81310, Malaysia

ARTICLE INFO

Keywords:
Remotely controlled actuation
Dynamic disulfide bonds
Carbon nanotubes
Shape changing performance
Self-healing effect

ABSTRACT

Smart materials can dynamically react to environmental stimuli and thus change at the micro or macro scale. However, when exposed to harsh conditions, damage can occur to them to varying degrees, thus affecting their performance and service life. In this study, a recyclable shape memory polyurethane material with self-healing properties was prepared using polycaprolactone (PCL) and polytetrahydrofuran diol (PTMG) as raw materials and isofuranone diisocyanate (IPDI) as a cross-linking agent. Dynamic cross-linking networks are constructed by introducing reversible disulfide bonds to enhance the self-healing and recyclable properties of the materials. Hydroxylated multiwalled carbon nanotubes (MWCNTs-OH), as photothermal particles, impart a remote response ability to the material, making the material temperature variable under near-infrared radiation (NIR). The shape memory recovery of CNT-PCL-PTMG can be triggered remotely and precisely controlled the irradiated NIR area. The results of tensile tests, scanning electron microscopy (SEM) and optical microscopy (OM) show that $^{3\%}$CNT-^{5}PCL-^{5}PTMG can achieve efficient and rapid self-healing. Additionally, the synergistic effect of transesterification and the dynamic exchange of disulfide bonds gives materials reprocessability for recycling use. The material is promising as an alternative material for soft robotics and smart sensors.

1. Introduction

Intelligent materials can dynamically respond to environmental stimuli after programming and thus change their motion microscopically or macroscopically [1,2]. Typical polymer-based programmable smart materials with their light weight, tailorable mechanical properties, and good processability make them highly compatible with work in the unstructured environments required by soft robots and smart actuators [3,4]. Shape-memory polymers (SMPs) are smart materials that can be deformed into a temporary shape and subsequently recover their initial shape when exposed to an external stimulus; therefore, they have good potential applications in the fields of industrial production, medical service and military reconnaissance [5,6].

Traditional SMPs consist of soft segments composed of low polar groups, such as semicrystalized polyester, and hard segments composed of strong polar and rigid groups (e.g., isocyanate), forming a microphase-separated structure [7]. For example, polyester-based chemically crosslinked SMPs can complete shape transformation under certain stimuli when the temperature rises to the crystallization melting temperature of the soft segment after shape programming under external forces in an amorphous state with oriented molecules [8,9]. However, when these materials are exposed to harsh conditions, damage can inevitably occur to varying degrees, thus affecting their performance and service life [10,11]. The spontaneous development of intelligent SMPs with controlled deformability and damage repair capability has become a critical issue. Inspired by the self-healing of damaged tissues by natural organisms, for the improvement of polymer reliability, reversible covalent bonds or noncovalent interactions such as Diels-Alder bonds [12], Schiff base bonds [13], hydrogen bonding [14] and metal-ligand interaction [15] were introduced to self-heal smart

* Corresponding author. Department of Biomedical Engineering, School of Big Health and Intelligent Engineering, Chengdu Medical College, Chengdu, 610500, China.
** Corresponding author.
*** Corresponding author.
E-mail addresses: chentao123@cmc.edu.cn (T. Chen), flyrain68@163.com (T. Zhang), liwang@cmc.edu.cn (L. Wang).

https://doi.org/10.1016/j.polymertesting.2023.108026
Received 2 February 2023; Received in revised form 23 March 2023; Accepted 12 April 2023
Available online 20 April 2023

materials. Compared to these bonds, disulfide bonds (DBs) can respond to external stimuli with dynamic exchange reactions due to their low bond energy [16,17]. Meanwhile, the dynamic character of DB may confer recyclability to materials [18]. To achieve a self-healing effect on a dynamic covalent shape-memory polyurethane (PU) network, a high mobility rate of the polymer chain is necessary to obtain macroscopic damage closure and dynamic chemical bond rebonding. Flexible polytetrahydrofuran (PTMG) with soft polymer chain structures have attracted much attention due to their faster chain mobility under thermal stimulation compared to other polyols [19]. However, most of the self-healing PTMG-based polyurethane presented poor mechanical properties and was unable to work under heavy loads [20]. To gain better mechanical properties, self-healing polyurethane was prepared from polycaprolactone glycol (PCL) due to its superior rheological and viscoelastic properties [21].

Conventional smart materials rely mostly on external stimulation to trigger their micro/macro movement changes [22,23]. Direct contact with the stimulating source for the initiation of shape changes has problems such as wasted energy and difficulty in precise regulation [24,25]. By applying an electric voltage/field or an alternating magnetic field, noncontact triggering could be approached, although they were highly dependent on the geometry of the samples and devices [26,27]. On the other hand, inspired by the light-driven mechanism in nature, photosensitive SMPs could capture the light signal and translate it into microscopic changes, showing fast macroscopic motion changes, and selectively heat the selected radiated area despite geometric limitations [25,28]. Hydroxylated multiwalled carbon nanotubes (MWCNTs-OH), as carbon-based nanomaterials with wideband optical absorption, exhibit a good photothermal conversion effect under near-infrared radiation (NIR) [29]. Surface-modified multiwalled carbon nanotubes (MWCNTs) effectively solved the problem of poor interfacial compatibility with polyurethane, while CNTs-OH introduced additional hydrogen bonds and enhanced the self-healing properties of materials.

In this study, semicrystalized poly (ϵ-caprolactone) (PCL) and elastic polytetrahydrofuran diol (PTMG) were selected as the soft segments of polyurethane (PU), and the hard segment was selected to be isophorone diisocyanate (IPDI). Damage healing under environmental stimuli was achieved by introducing 4-aminophenyl disulfide (DTDA) into the cross-linked network. The effect of the introduced MWCNTs-OH on the photothermal effect and physio-chemical properties of the material was also investigated by controlling the mass fraction of the introduced MWCNTs-OH. Furthermore, the prepared materials were programmed and recovered by bending experiments under direct heating from oven, indirect heating by NIR. The self-healing efficiency of the samples was evaluated by stretching, and the self-healing effect was analyzed by scanning electron microscopy (SEM) and optical microscopy (OM). Finally, the recyclability of the materials was evaluated by process into different shapes. The material is promising as an alternative material for soft robotics and smart sensors.

2. Experimental

2.1. Materials

Polytetrahydrofuran diol (PTMG, M_n = 3000 g/mol) and polycaprolactone glycol (PCL, M_n = 2000 g/mol) were purchased from Jining Hua Kai Resin Co., Ltd, Jining, China. Isophorone diisocyanate (IPDI, >99%) and tin 2-ethylhexanoate ($C_{16}H_{30}O_4Sn$, >95.0%) were purchased from Aladdin Chemical Reagent Factory, Shanghai, China. Beijing Innochem Technology Co. provided 4-aminophenyl disulfide (DTDA). MWCNTs-OH (>98%) were purchased from Jiazhao Ye Advanced Materials Co., Ltd. The length is 2–8 μm, the outer diameter is 10–15 nm, and the inner diameter is 5–8 nm.

2.2. Preparation of composite materials

Fig. 1a shows the synthetic route of the composite materials. The melted PCL and PTMG were added to a three-necked flask at a mass ratio of 50 to 50, and MWCNTs-OH was added at a certain weight ratio and sonicated for 1 h. Subsequently, IPDI and a few drops of tin 2-ethylhexanoate were added to the mixed solution and allowed to stir at 200–300 r/min at 70 °C for 2 h of reaction. After the prepolymer was prepared, the reaction temperature was lowered to 40 °C, DTDA (dissolved in dichloromethane in advance) was added for chain extension, and stirring was continued for 2 h. It was then transferred to a tetrafluoroethylene mold and cured at 90 °C for 24 h. The preparation process was carried out in a nitrogen atmosphere. The molar ratio of PTMG/PCL (-OH): DTDA (S–S): IPDI (-NCO) was 2:1:3. The composites without MWCNTs-OH were first prepared, and the effects of different mass ratios of PCL and PTMG on their shape memory and self-healing were investigated. The prepared composite material was ^{x}PCL-^{y}PTMG. The superscript "x" stands for PCL weight content, and the superscript "y" stands for PTMG weight content. To investigate the effect of MWCNTs-OH on the material properties, different materials were prepared by controlling the mass fraction of embedded MWCNTs-OH. The prepared composite material was $^{z\%}$CNT-^{5}PCL-^{5}PTMG. The superscript "z" stands for MWCNT-OH weight content.

2.3. Characterization

X-ray diffraction (XRD) (DX-2700, China Fangyuan Instrument Co., Ltd., China) was used to perform the material phase analysis on different materials. Fourier transform infrared spectrometry (FTIR) was performed on a TENSOR-27 (Bruker, Bremen, Germany) in the wavenumber range of 400 cm^{-1} – 4000 cm^{-1}. The component content of the composite materials was analyzed by thermogravimetric analysis (TGA) on a Netzsch DSC-204F1 thermal analyzer from SELB in Germany. To evaluate the thermal properties of the materials, tests were performed using a differential scanning calorimeter (DSC, Netzsch DSC-204F1) with a temperature rise rate of 10 K/min. The samples were cut into 15 mm × 15 mm × 2 mm slices, and the water contact angles were measured at the top and bottom (surface in contact with air and surface in contact with the bottom of the Teflon mold) using a contact angle meter (SDC 200, Yuding Precision Instrument Co., Ltd., China). The samples were cut into sheets (10 mm × 10 mm × 2 mm), and field emission scanning electron microscopy (FE-SEM, INSPECTF50, FEI, Eindhoven, Holland) equipped with X-ray energy dispersive spectroscopy (EDS) was used to observe the micromorphology and elemental composition of the materials. The different samples were cut into blocks of 10 mm × 10 mm × 3 mm size, and the original weight was recorded as W_1; subsequently, they were immersed in ethyl acetate for 12 h. The samples were removed, and the wet weight was recorded as W_2. The samples were dried, and the dry weight was recorded as W_3. The gel content (G) and degree of swelling (D) rate were calculated according to the following formulas.

$$G\,(\%) = \frac{W_3}{W_1} \times 100\% \tag{1}$$

$$D\,(\%) = \frac{W_2}{W_1} \times 100\% \tag{2}$$

The thermomechanical properties of the sample (20 mm × 2 mm × 1 mm) were investigated with a dynamic mechanical analyzer DMA (DMA1, Mettler Toledo) with a heating rate of 3 K/min from −50 °C to 80 °C and an amplitude of 0.2% at a frequency of 1 Hz.

To investigate the effect of MWCNTs-OH content on the photothermal effect of the samples, the samples were irradiated using a near-infrared laser transmitter (HW808AD2000-34F, Shenzhen Infrared Laser Technology Co., Ltd, China). The irradiation distance was 0.3 m, and the spot size was 2 cm. The samples were cut into 10 mm × 10 mm

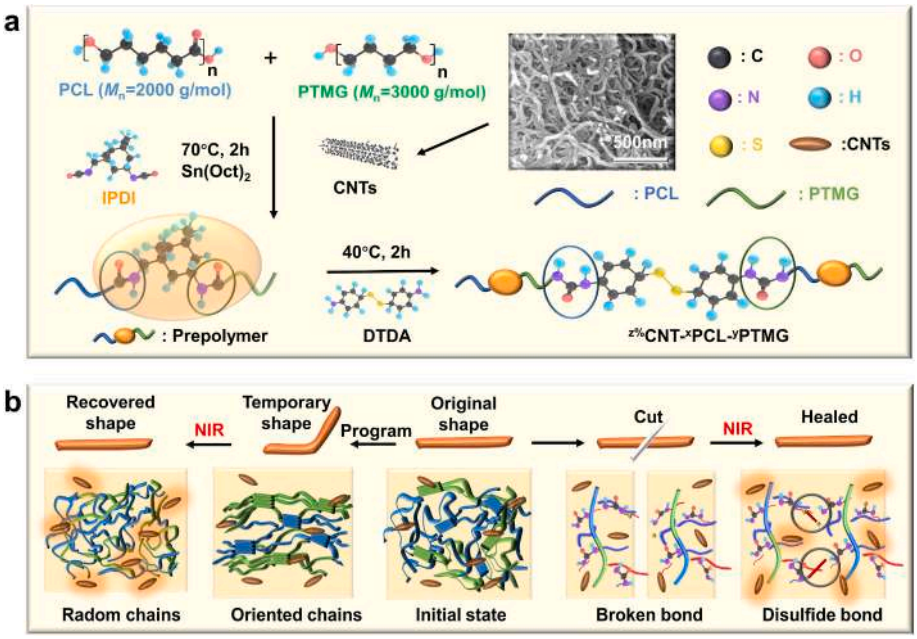

Fig. 1. (a) Synthetic route of $^{z\%}$CNT-^{x}PCL-^{y}PTMG (b) shape memory and self-healing mechanism of $^{z\%}$CNT-^{x}PCL-^{y}PTMG.

× 2 mm sheets and irradiated by NIR light at 0.2 W/cm^2. The temperature changes of the samples were recorded by a thermal imaging camera (UTi260B, Uni-Trend Technology Co., Ltd, China). According to the instructions, the observation distance was 0.25 m and the irradiance was set to 0.94.

The prepared material presents a shape memory effect which recovers from the programmed orientation state to the initial random state (Fig. 1b). The shape memory behaviors of different samples were examined with bending experiments. The different samples were cut into 25 mm × 10 mm × 2 mm pieces and heated at 50 °C in an oven to fold them to 90°. The samples were subsequently shape fixed at 0 °C, and the fixation angle of the sample was recorded as θ_1. Finally, the samples were heated in different ways to reach the temperature of the shape memory transition switch, and the angle of the final recovery was recorded as θ_2 (Specifically, the initial straight shape is 180°, and the programmed bending shape is 90°). The shape fixation rate (R_f) and shape recovery rate (R_r) were calculated according to Formulas (3) and (4).

$$\text{Shape fixation rate } (\%) = \frac{180 - \theta_1}{90} \times 100\% \quad (3)$$

$$\text{Shape recovery rate } (\%) = \frac{\theta_2 - 90}{90} \times 100\% \quad (4)$$

Due to the introduction of dynamic disulfide bonds, the material has the ability to self-heal damage (Fig. 1b). The mechanical properties and self-healing efficiency of the composites were measured by an electronic universal testing machine (MIT-30kN, Changzhou SFMIT Instrument Co., Ltd., China). The size of the samples was 25 mm × 10 mm × 2 mm and had a tensile speed of 5 mm/min. The self-healing efficiency was calculated using the following formula.

$$\text{Self} - \text{healing efficiency } (\%) = \frac{\text{tensile strain (healed)}}{\text{tensile strain (original)}} \times 100\ \% \quad (5)$$

The self-healing of $^{3\%}$CNT-^{5}PCL-^{5}PTMG was observed using optical microscopy (OM, Xuzhou Leyue Safety Technology Co., Ltd.), physical photos, and SEM.

The sample was sheared into pieces and then heated at high temperature to be remodeled into different shapes in the polytetrafluoroethylene mold. Where, the "tree" model is 30 mm × 30 mm × 3 mm; 3D "rabbit" model is 57 mm × 36 mm × 35 mm.

3. Results and discussion

3.1. Characterization of polymeric PCL-PTMG

To design shape memory materials with highly efficient self-healing effect, IPDI with a lower steric hindrance structure was chosen as a hard segment to improve the migration rate of polymer chains. The dynamic network was constructed by introducing disulfide bonds to enhance the self-healing effect of the material. First, ^{x}PCL-^{y}PTMG was prepared, and the effects of different raw material ratios on shape memory and self-healing performance were explored. Fig. 2a showed the FTIR pattern of ^{x}PCL-^{y}PTMG. The vibrational absorption peak of the benzene ring backbone of DTDA at 1594 cm^{-1} indirectly confirmed the introduction of disulfide bonds. The appearance of carbamate bonds represented the formation of PU [30]. The peak of the –NCO group at approximately 2210–2250 cm^{-1} was not observed for all samples, indicating that the reaction was complete without residual IPDI [31]. Fig. 2b showed the gel content and degree of swelling of ^{x}PCL-^{y}PTMG. As the mass fraction of PCL increased, the degree of swelling of the material increased from 242.7% to 411.3%. All samples had a high gel content (>80%), which ensured the stability of the cross-linked network. The results indicated that PU was successfully synthesized. The shape-programmed samples were exposed to an oven at 50 °C to evaluate their shape memory properties [32]. Fig. 2c show the shape recovery process. As the mass fraction of PTMG increased, the shape fixation rate of the samples gradually decreased, and the shape recovery rate gradually increased (Fig. S1). Fig. 2d showed the molecular dynamics simulation results of ^{x}PCL-^{y}PTMG. Herein, the cohesive energy densities (CED) were calculated by the COMPASS force field. All models showed that the CED value exceeded 200 kJ/mol, which indicated that the material showed good mechanical properties. In particular, as the mass fraction of PTMG increased, the CED value of the material gradually increased. This was attributed to the van der Waals forces in the PU network units which increased and the self-healing properties improved. In general, the increase in crosslinking led to an increasing of the self-healing temperature of materials and reduced the self-healing efficiency [33]. Considering the results of the bending experiments, ^{5}PCL-^{5}PTMG was selected for self-healing property testing. Fig. 2e shows SEM photos of

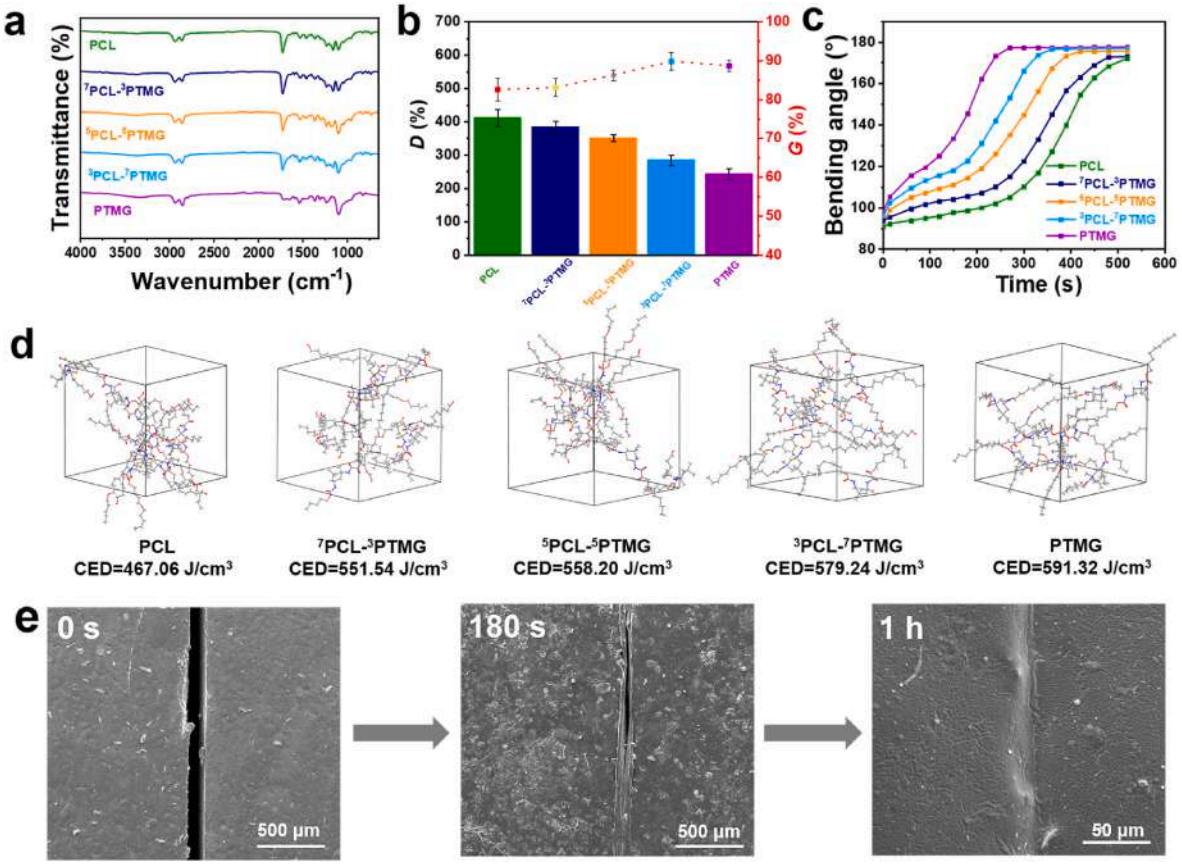

Fig. 2. (a) FTIR curves of ^{x}PCL-^{y}PTMG, (b) Gel content and degree of swelling of ^{x}PCL-^{y}PTMG, (c) bending angle with time curve of the shape recovery process for ^{x}PCL-^{y}PTMG, (d) A snapshot of an all-atom molecular dynamic simulation of ^{x}PCL-^{y}PTMG (the bat model emphasizes the hard part), (e) SEM photo of the ^{5}PCL-^{5}PTMG self-healing process (scale bar of 0 s and 180 s: 500 μm, scale bar of 1 h: 50 μm).

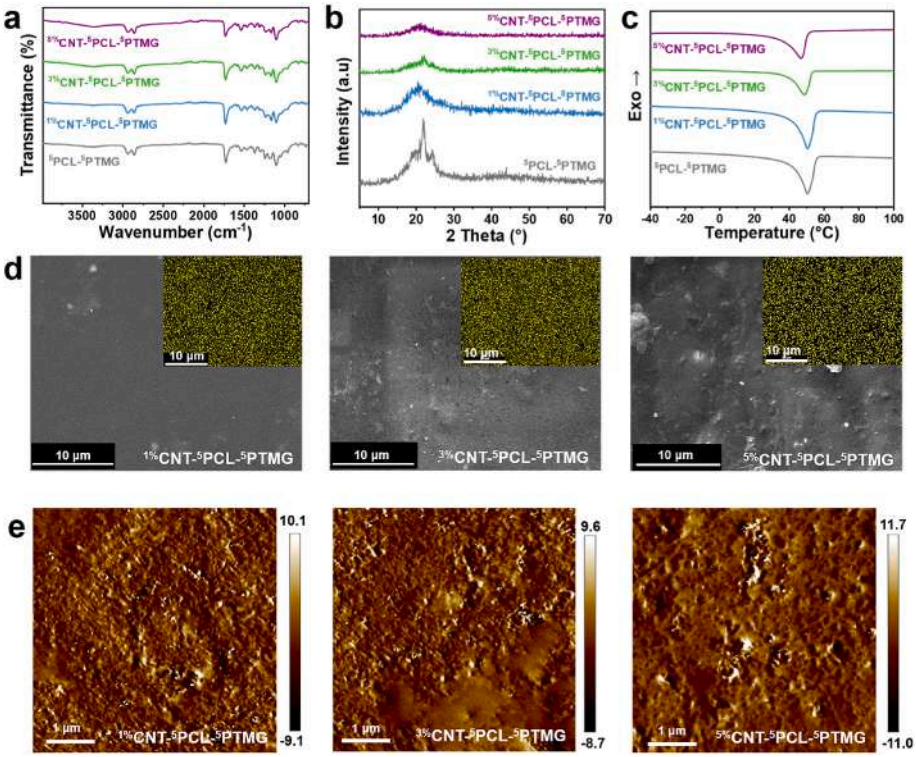

Fig. 3. Physio-chemical properties of (a) FTIR spectra, (b) XRD curves, (c) DSC curves, (d) SEM and EDS photos (scale bar: 10 μm), (e) AFM photos (scale bar: 1 μm).

^{5}PCL-^{5}PTMG during different self-healing processes at 50 °C. The cracks on the surface of the sample started to close at 180 s. After 1 h, only a few traces could be seen on the SEM. On balance, ^{5}PCL-^{5}PTMG was selected for subsequent testing due to its high self-healing and shape memory properties.

3.2. Physio-chemical properties of CNT-PCL-PTMG composites

Traditional self-healing materials present poor mechanical properties [34]. In this study, the mechanical properties of the material were enhanced while giving the material the ability to respond remotely. MWCNTs-OH were embedded into ^{5}PCL-^{5}PTMG. The effects of different mass fractions of MWCNTs-OH on the physio-chemical properties, shape memory properties and self-healing properties of the materials were investigated. Detailed information about the material properties, i.e., crystalline properties, SEM photos of MWCNTs-OH, water contact angle, degree of swelling, and gel content of the network materials were provided in the supporting information (Figs. S2–S5, Tables S1–S2). Fig. 3a shows the FTIR pattern of $^{z\%}$CNT-^{5}PCL-^{5}PTMG. All the curves exhibited similar trends. There was a broad absorption peak at 3339 cm^{-1}, represented by *N*-H groups, and the characteristic peak located at 1730 cm^{-1} was caused by the C=O bond stretching vibration, which indicated that the carbamate bond had been formed. In addition, the peak of the –NCO group around 2250 cm^{-1} was not observed, indicating that the reaction is complete. After Fourier self-deconvolution of the C=O band, some additional bands appeared (Table S3 and Fig. S6) which proved the existence of hydrogen bonds in polyurethane composites. The gel content and degree of swelling tests showed that the samples had a high crosslink density, which ensured the stability of the network. As the mass fraction of MWCNTs-OH increased, the hydrophilicity of the material gradually increased. Interestingly, the difference between the water contact angle measured at the top and bottom of the material was not significant, which proves that the MWCNTs-OH did not accumulate/precipitate during the preparation process. The introduction of MWCNTs-OH resulted in a gradual decrease in the intensity of the peaks in XRD (Fig. 3b), representing a decrease in the crystalline properties. The DSC curves of $^{z\%}$CNT-^{5}PCL-^{5}PTMG were shown in Fig. 3c. The T_m of -^{5}PCL-^{5}PTMG was 50.74 °C. When the mass fraction of MWCNTs-OH increased to 5%, T_m decreased to 47.08 °C. With the introduction of more mass fractions of MWCNTs-OH, the arrangement of polymer chain segments in a regular structure was hindered, and the crystallization behavior of the polymer was destroyed.

Fig. 3d shows the SEM and EDS photos of $^{z\%}$CNT-^{5}PCL-^{5}PTMG. All samples exhibited a uniform distribution of S elements. Combined with the gel content and FTIR test, a dynamic covalent crosslinked network was formed. This result indicated that the material could achieve self-healing by breaking and rebonding dynamic disulfide bonds. The surface of ^{5}PCL-^{5}PTMG was smooth, and the surface of the samples became rough as the mass fraction of MWCNTs-OH increased. In addition, the MWCNTs-OH did not show significant agglomeration in any of the samples. The cause may be attributed to the better interfacial compatibility of the modified CNTs with the polyurethane matrix. The uniform distribution of MWCNTs-OH in the matrix facilitates the remote control of the temperature of the material under NIR irradiation. $^{z\%}$CNT-^{5}PCL-^{5}PTMG was observed in phase mode by using AFM (Fig. 3e), exhibiting a clear microphase separation structure. The bright areas representing the hard segments and the dark areas representing the soft segments diffuse into each other. Compared to ^{5}PCL-^{5}PTMG (Fig. S7), the sample after the introduction of MWCNTs-OH exhibited a more obvious structure of microphase separation. An excellent microphase separation structure is necessary for the material to achieve shape memory and self-healing.

3.3. Shape memory performance of $^{z\%}$CNT-^{5}PCL-^{5}PTMG

According to the enthalpies and crystallization results, all $^{z\%}$CNT-^{5}PCL-^{5}PTMG samples presented certain degree of crystallinity, which implies that shape memory effect could be achieved by using T_m as a transition switch. Specifically, at temperatures lower than T_ms, PCL and PTMG are in the crystalline state, and the polymer chains remain frozen. When the temperature is higher than T_ms, the polymer chains can be programmed to be oriented under extra stress. Subsequently, after cooling the shape-fixed sample lower than T_ms, the polymer chains are directionally crystallized to form a temporary shape. When the temperature is again higher than T_ms, the material recovers to its original shape due to an increase in entropy. Fig. 4d showed the shape memory transition process of $^{z\%}$CNT-^{5}PCL-^{5}PTMG at 50 °C. The recovery speed and shape recovery rate of the samples decreased with increasing mass fraction of MWCNTs-OH. This is attributed to the introduction of MWCNTs-OH destroying the crystallinity of the materials. Fig. 4b statistically shows the shape recovery rate and shape fixation rate of different samples in the bending experiment at 50 °C. The materials still have a high shape fixation rate (>80%) and shape recovery rate (>84%) despite the introduction of additional filler. It is noteworthy that the shape fixation rate of $^{3\%}$CNT-^{5}PCL-^{5}PTMG is slightly lower than that of the other samples, which may be related to the lower gel content of the material. MWCNTs-OH could capture near-infrared light signals and generate heat. The effect of different mass fractions of MWCNTs-OH on the temperature change of the material under NIR irradiation with a power of 0.2 W/cm^2 was investigated (Fig. 4a). Fig. 4c showed the remote heating of different samples using NIR to trigger their shape recovery. Due to the higher mass fraction of MWCNTs-OH, $^{5\%}$CNT-^{5}PCL-^{5}PTMG had the fastest change in bending angle. Fig. 4e illustrateed the thermal infrared photos of different samples reaching the saturation temperature under NIR irradiation with a power of 0.2 W/cm^2. The saturation temperature of NIR irradiation of $^{1\%}$CNT-^{5}PCL-^{5}PTMG was close to that of direct heating for bending experiments (50 °C), so $^{1\%}$CNT-^{5}PCL-^{5}PTMG was selected for NIR-induced bending experiments compared with direct heating (Video S1). The temperature of $^{1\%}$CNT-^{5}PCL-^{5}PTMG increased faster and uniformly due to the uniformly distributed photothermal conversion particles forming a thermal conductivity network within the matrix. This led to a faster shape recovery speed under NIR irradiation than under direct heating. Additionally, the part of the material that was directly irradiated by NIR generated a large amount of heat, which provided the necessary conditions for NIR to precisely trigger its micro/macroscopic changes.

Supplementary video related to this article can be found at https://doi.org/10.1016/j.polymertesting.2023.108026

3.4. Self-healing effect of $^{z\%}$CNT-^{5}PCL-^{5}PTMG

To enhance the self-healing efficiency and prolong the service life of the material, disulfide bonds were introduced to construct dynamic covalent networks. Considering the low reactivity of 4,4′-disulfanediyldiphenol (DTDP) and the susceptibility of (2-(4-aminophenyl)-1,3,2-dioxaborolan-4-yl) methanethiol (SBN) to cracking, DTDA was chosen as the chain extender [35]. After the materials were employed as precision devices, the self-healing properties could be triggered by direct heating, which may disrupt the normal use of other components. In contrast, by introduction of MWCNTs-OH, self-healing polyurethanes could be triggered without external heating. At the same time, the modified CNTs increased the hydrogen bonding density of the material and built a physical cross-linked network, which further enhanced the mechanical properties and self-healing properties [36]. Fig. 5d showd the mechanical properties and self-healing efficiency of $^{3\%}$CNT-^{5}PCL-^{5}PTMG. The rigid benzene ring in DTDA ensures the mechanical properties of the material. Meanwhile, MWCNTs-OH as the reinforcing phase improve the mechanical properties of the material. Fig. S8 summarizes the mechanical properties and self-healing efficiency of $^{z\%}$CNT-^{5}PCL-^{5}PTMG. With the increase in the mass fraction of MWCNTs-OH, the tensile strength modulus of the material was gradually enhanced, and the elongation at break gradually decreased. Fig. 5a

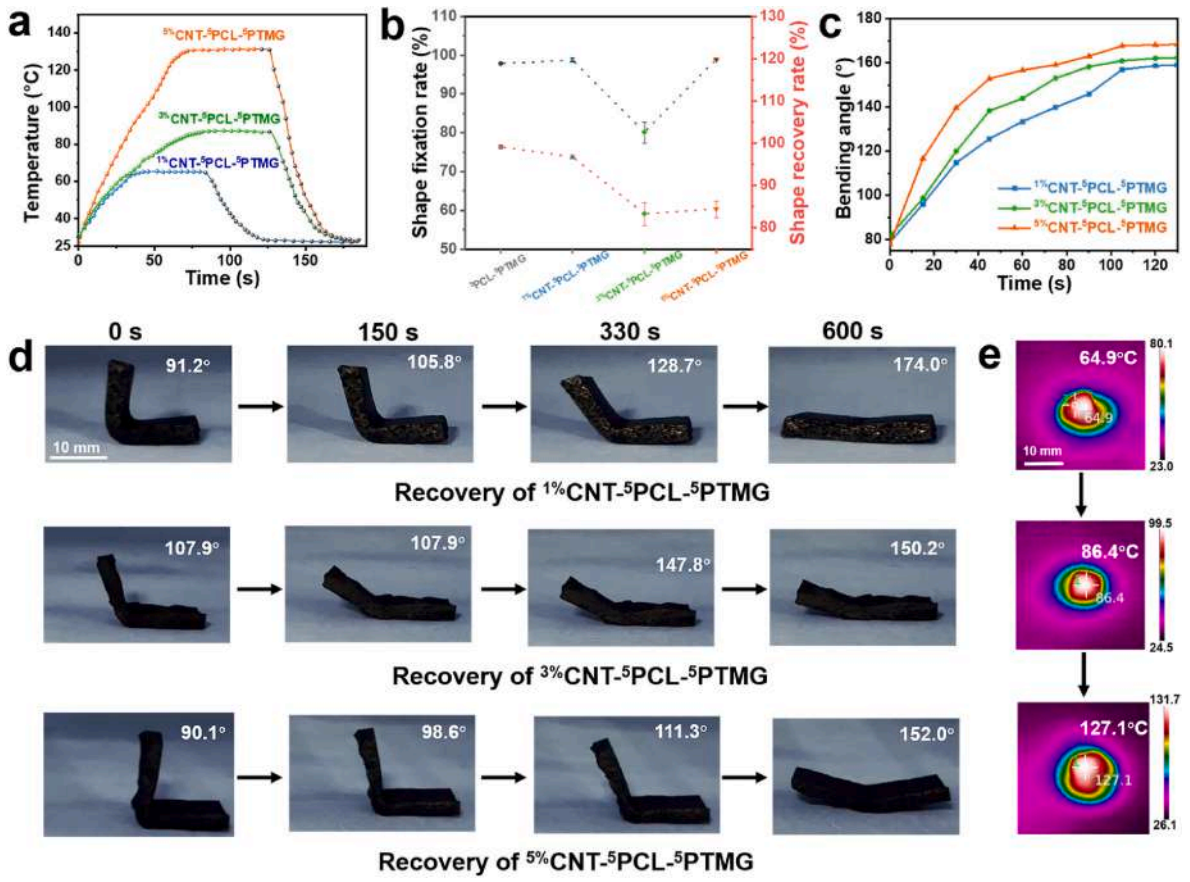

Fig. 4. (a) Temperature change curve of $^{z\%}$CNT-^{5}PCL-^{5}PTMG heated to saturation temperature using NIR with a power of 0.2 W/cm^2, (b) Shape fixation rate and shape recovery rate of samples in the bending experiment, (c) The change in bending angle of $^{z\%}$CNT-^{5}PCL-^{5}PTMG irradiated by NIR with a power of 0.2 W/cm^2, (d) Visual demonstration of shape memory for $^{z\%}$CNT-^{5}PCL-^{5}PTMG in a 50 °C oven (scale bar: 10 mm), (e) Thermal infrared photos of samples reaching saturation temperature under NIR irradiation with a power of 0.2 W/cm^2 (scale bar: 10 mm).

showd a visual demonstration of $^{3\%}$CNT-^{5}PCL-^{5}PTMG being cut and healed at 60 °C. The scratches on the sample surface largely disappeared after heating in an oven at 60 °C for 3 h. Moreover, the SEM image of the self-healing of the cracked sample confirmed the healing process (Fig. 5b). After heating in the oven at 60 °C for 3 h, only rough traces were observed on the surface of the samples. The material was cracked under external forces, and the reversible dynamic covalent bonding was broken. As the temperature increased, the storage modulus of the sample decreased (the DMA curve in Fig. S9 verified this conclusion), and the polymer chain segments start to move. The damaged surfaces diffused into each other, and the broken dynamic disulfide bonds rebond, allowing the damage to begin to close. Notably, MWCNTs-OH followed the polymer chains to move toward the damage, increasing the hydrogen bonding density at the damage. The rebonding of hydrogen bonds improved the self-healing efficiency.

To demonstrate the self-healing ability, $^{3\%}$CNT-^{5}PCL-^{5}PTMG was subjected to three self-healing (60 °C, 3 h) cycles, and the sample was able to lift a 3 kg dumbbell (Fig. 5e). Fig. 5c and Video S2 show the self-healing performance of $^{3\%}$CNT-^{5}PCL-^{5}PTMG triggered by NIR observed using optical microscopy. Under NIR irradiation with a power of 0.2 W/cm^2, the storage modulus of the sample decreased, and the damage began to heal (90 s). As the irradiation time increased, the temperature continued to rise, and a large number of mobile polymer chains and disulfide bonds underwent an exchange reaction accompanied by hydrogen bond reorganization (120 s). When the sample cooled down, there was just a scratch on the sample surface. Such rapid self-healing behavior could be attributed to the excellent photothermal effect of MWCNTs-OH, which changed the temperature locally and precisely under NIR irradiation. Due to the good dispersion of the photothermal particles in PU, the heat spreaded rapidly, resulting in a uniform and rapid increase in the material temperature.

Supplementary video related to this article can be found at https://doi.org/10.1016/j.polymertesting.2023.108026

3.5. *Recyclability of $^{z\%}$CNT-^{5}PCL-^{5}PTMG*

The introduction of dynamic covalent bonding gives the specially designed PU the potential to be recyclable at high temperatures. As illustrated in Fig. 6a, the material will undergo transesterification under high temperature and residual catalyst conditions, causing topological changes in the network [37]. $^{5\%}$CNT-^{5}PCL-^{5}PTMG can reach 130 °C under NIR irradiation with a power of 0.2 W/cm^2, which was sufficient to trigger the recyclability of the material. Fig. 6b shows the shape memory performance of the reprocessed sample. After two cycles, the shape fixation rate of the sample remained at a high level (>96%). The slight increase in shape recovery of the samples after the first recycling might be related to the removal of internal stress and the sustained response of the PU. Fig. 6c shows the reshaped model picture and the physical display photos. The samples can still be reprocessed according to the shape of the model after several cycles, which implies a better recycling potential of the materials we prepared to avoid resource waste.

Further NIR responsive demonstration of precisely remote-controlled shape-changing performance were carried with samples of various shapes. Fig. 7a and Video S3 show the shape recovery of the left and right parts of the "tree" precisely triggered by the irradiation. When the left and right parts of the sample were irradiated separately, the shape of the corresponding part of the sample was recovered rapidly. However, because the MWCNTs-OH formed a uniform thermal conductivity

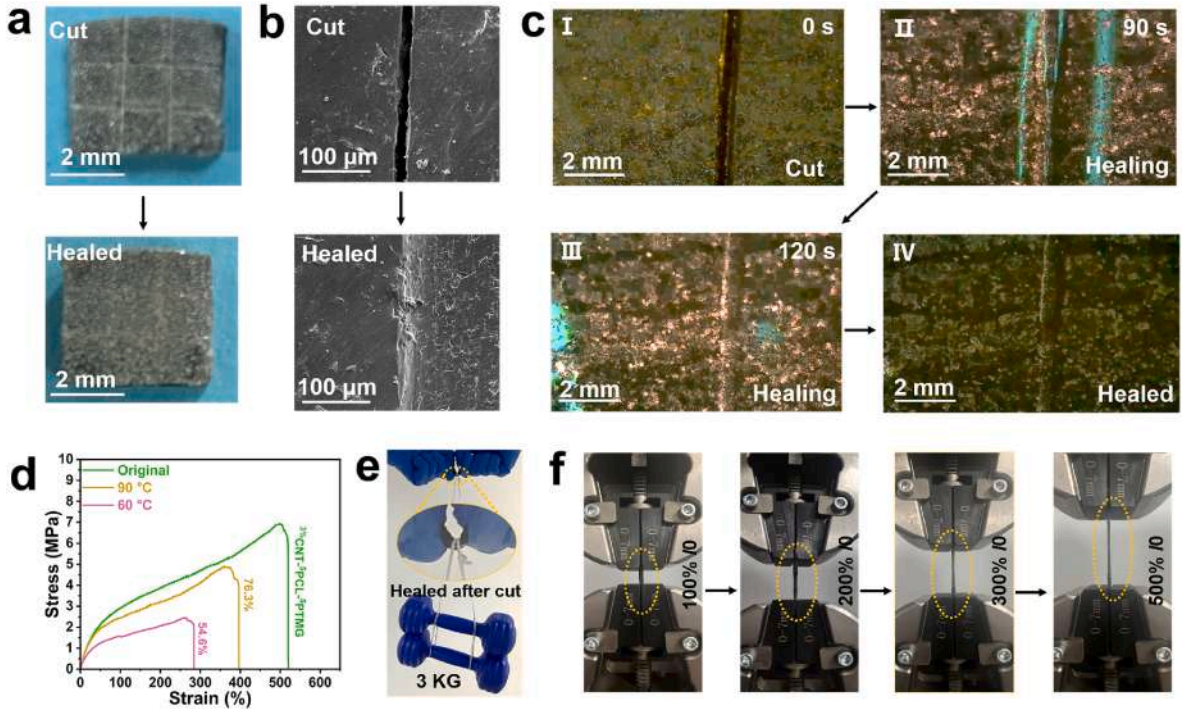

Fig. 5. (a) Visual demonstration of $^{3\%}$CNT-^{5}PCL-^{5}PTMG being cut and healed at 60 °C, (b) SEM photos of $^{3\%}$CNT-^{5}PCL-^{5}PTMG after cutting and SEM photos after self-healing at 60 °C (scale bar: 100 μm), (c) Optical photographs of $^{3\%}$CNT-^{5}PCL-^{5}PTMG for NIR-induced self-healing (scale bar: 2 mm), (d) Mechanical properties of $^{3\%}$CNT-^{5}PCL-^{5}PTMG and self-healing efficiency of healing at different temperatures for 3 h, (e) Photo of $^{3\%}$CNT-^{5}PCL-^{5}PTMG lifting a 3 KG dumbbell after 3 h of healing at 60 °C, (f) Visual demonstration of $^{3\%}$CNT-^{5}PCL-^{5}PTMG in the stretching process.

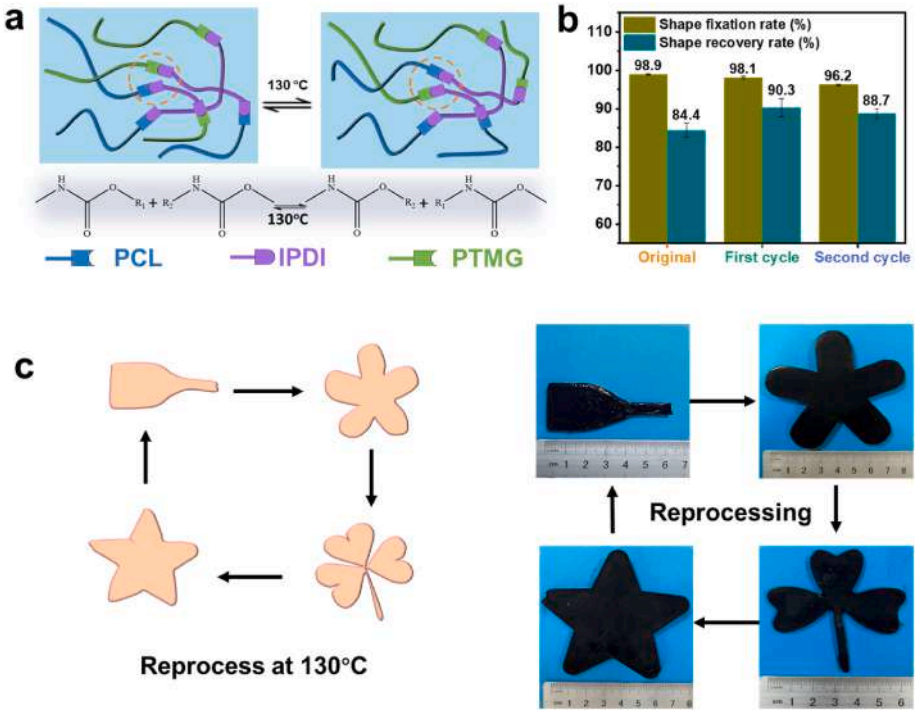

Fig. 6. (a) Transesterification mechanism; (b) Line graph of the shape fixation rate and shape recovery rate after$^{5\%}$CNT-^{5}PCL-^{5}PTMG recycling; (c) Model pictures and physical photos of different shapes of $^{z\%}$CNT-^{5}PCL-^{5}PTMG after high-temperature recycling.

network, the heat was able to diffuse rapidly, causing the shape of the left half to begin to recover as well, but the recovery rate of the left half was much lower than that of the right half of the sample. To further verify the shape memory properties of the NIR light remotely/precisely triggered material, $^{1\%}$CNT-^{5}PCL-^{5}PTMG was made into a larger size model to avoid rapid thermal conduction. As shown in Fig. 7b and Video S4, the "clover" that has been shape-programmed was irradiated with NIR to trigger its shape recovery. As shown in the thermal imaging photos, the temperature of the part irradiated by NIR increases rapidly, while the temperature of the part not irradiated remains largely

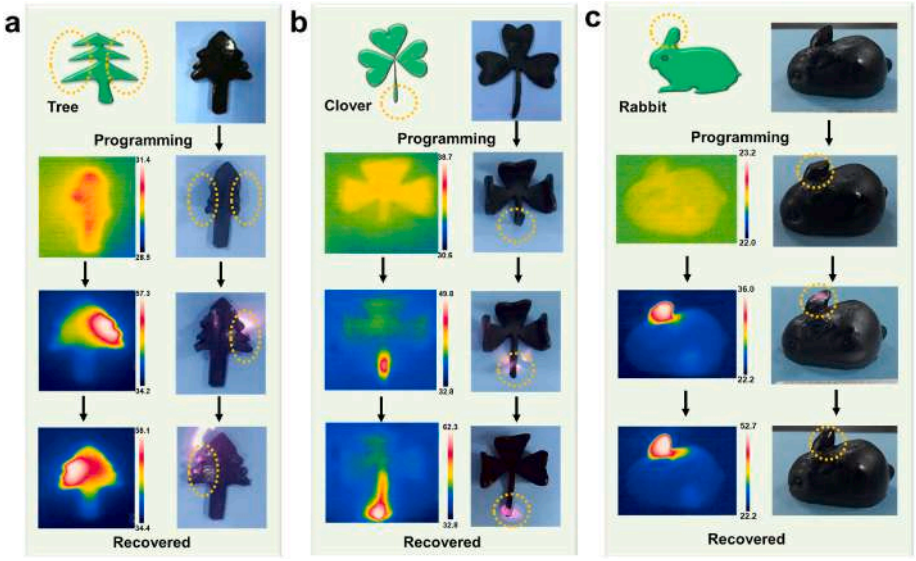

Fig. 7. Model of samples, optical and thermographic photos of the shape recovery process of samples after shape programming: (a) "tree", (b) "clover", and (c) "rabbit".

unchanged. As shown in Fig. 7c, the sample was prepared as a 3D rabbit model. After shape programming, "the rabbit ears" were bent. After NIR irradiation, the rabbit's ears were re-erected. The shape recovers quickly when the temperature reaches the shape memory switch. The precise and fast NIR-induced shape memory recovery will greatly expand the applications of our prepared samples in soft robotics, smart actuators, and other fields.

Supplementary video related to this article can be found at https://doi.org/10.1016/j.polymertesting.2023.108026

4. Conclusions

In this study, NIR-responsive shape memory polyurethane composites with self-healing and recyclable properties were developed. These dynamic cross-linked networks were constructed by introducing a reversible disulfide bond. MWCNTs-OH acted as a reinforcing phase to enhance the mechanical properties of the material functioning as a photothermal converter to support the material with remotely responsive capabilities. SEM photographs and water contact angle tests showed that MWCNTs-OH were homogeneously dispersed in the matrix. The $^{z}_{\%}$CNT-^{5}PCL-^{5}PTMG exhibited controlled temperature changes under NIR irradiation at a power of 0.2 W/cm^2. The shape memory recovery of $^{1\%}$CNT-^{5}PCL-^{5}PTMG can be triggered remotely and precisely by controlling the irradiated NIR area. Tensile experiments demonstrated that $^{z}_{\%}$CNT-^{5}PCL-^{5}PTMG exhibited excellent self-healing efficiency at 60 °C. The NIR remotely triggering the transesterification of $^{z}_{\%}$CNT-^{5}PCL-^{5}PTMG showed the composite networks with excellent multiple recyclability. Combined with the comprehensive properties of these composites, this light responsive smart networks has a promising future in soft robots, smart actuators, and similar applications.

Funding

This research was funded by Sichuan Science and Technology Program (2021YFH0098, 23ZDYF0634) and the Joint Scientific Research Fund of Chengdu Medical College - People' Hospital of Chengdu Pidu District (202lLHPJ-03).

Authors' contributions

Xiaohu Chen did writing and original draft preparation. Li Wang was responsible of writing, reviewing and editing. Tao Chen did the methodology. Tuck Waye Wong and Ting Zhang were responsible for Software. Junfeng Li and Yonggui Liu did the data curation.

Declaration of competing interest

The authors declare that they have no known competing financial interests or personal relationships that could have appeared to influence the work reported in this paper.

Data availability

No data was used for the research described in the article.

Appendix A. Supplementary data

Supplementary data to this article can be found online at https://doi.org/10.1016/j.polymertesting.2023.108026.

References

[1] L. Hu, Q. Zhang, X. Li, M.J. Serpe, Stimuli-responsive polymers for sensing and actuation, Mater. Horiz. 6 (9) (2019) 1774–1793, https://doi.org/10.1039/c9mh00490d.
[2] Y.N. Kim, K.H. Nam, Y.C. Jung, H. Han, Interfacial adhesion and self-healing kinetics of multi-stimuli responsive colorless polymer bilayers, Compos. B Eng. 203 (2020), 108451, https://doi.org/10.1016/j.compositesb.2020.108451.
[3] Q.C. Zheng, C.X. Xu, Z.L. Jiang, M. Zhu, C. Chen, F.F. Fu, Smart actuators based on external stimulus response, Front. Chem. 9 (2021), 650358, https://doi.org/10.3389/fchem.2021.650358.
[4] H. Son, C. Yoon, Advances in stimuli-responsive soft robots with integrated hybrid materials, Actuators 9 (4) (2020) 115, https://doi.org/10.3390/act9040115.
[5] M.C. Biswas, S. Chakraborty, A. Bhattacharjee, Z. Mohammed, 4D printing of shape memory materials for textiles: mechanism, mathematical modeling, and challenges, Adv. Funct. Mater. 31 (19) (2021), 2100257, https://doi.org/10.1002/adfm.202100257.
[6] A. Lendlein, M. Balk, N.A. Tarazona, O.E.C. Gould, Bioperspectives for shape-memory polymers as shape programmable, Active Materials, Biomacromolecules 20 (10) (2019) 3627–3640, https://doi.org/10.1021/acs.biomac.9b01074.
[7] L. Wang, X.H. Chen, X.Y. Zeng, K. Luo, S.Y. Zhou, P.C. Zhang, J.F. Li, Degradable smart composite foams for bone regeneration, Compos. Sci. Technol. 217 (2022), 109124, https://doi.org/10.1016/j.compscitech.2021.109124.
[8] A. Gupta, A. Maharjan, B.S. Kim, Shape memory polyurethane and its composites for various applications, Appl. Sci.-Basel 9 (21) (2019) 4694, https://doi.org/10.3390/app9214694.
[9] M.A. Gorbunova, D.V. Anokhin, E.R. Badamshina, Recent advances in the synthesis and application of thermoplastic semicrystalline shape memory polyurethanes, POLYM SCI SER B+ 62 (5) (2020) 427–450, https://doi.org/10.1134/s1560090420050073.

[10] F. Wang, W.T. Wang, C. Zhang, J.N. Tang, X.R. Zeng, X.J. Wan, Scalable manufactured bio-based polymer nanocomposite with instantaneous near-infrared light-actuated targeted shape memory and remote-controlled accurate self-healing, Compos. B Eng. 219 (2021), 108927, https://doi.org/10.1016/j.compositesb.2021.108927.
[11] M. Khatib, O. Zohar, H. Haick, Self-healing soft sensors: from material design to implementation, Adv. Mater. 33 (11) (2021), 2004190, https://doi.org/10.1002/adma.202004190.
[12] L.B. Feng, X. He, Y.P. Zhang, D.G. Qu, C.S. Chai, Triple roles of thermoplastic polyurethane in toughening, accelerating and enhancing self-healing performance of thermo-reversible epoxy resins, J. Polym. Environ. 29 (3) (2021) 829–836, https://doi.org/10.1007/s10924-020-01923-4.
[13] H.L. Chen, J.W. Cheng, L.X. Ran, K. Yu, B.T. Lu, G.Q. Lan, F.Y. Dai, F. Lu, An injectable self-healing hydrogel with adhesive and antibacterial properties effectively promotes wound healing, Carbohydr. Polym. 201 (2018) 522–531, https://doi.org/10.1016/j.carbpol.2018.08.090.
[14] M. Wei, M.Q. Zhan, D.Q. Yu, H. Xie, M.J. He, K.K. Yang, Y.Z. Wang, Novel poly (tetramethylene ether)glycol and poly(epsilon-caprolactone) based dynamic network via quadruple hydrogen bonding with triple-shape effect and self-healing capacity, ACS Appl. Mater. Interfaces 7 (4) (2015) 2585–2596, https://doi.org/10.1021/am507575z.
[15] Y.Y. Han, X.D. Wu, X.X. Zhang, C.H. Lu, Self-healing, highly sensitive electronic sensors enabled by metal-ligand coordination and hierarchical structure design, ACS Appl. Mater. Interfaces 9 (23) (2017) 20106–20114, https://doi.org/10.1021/acsami.7b05204.
[16] L.R. Tian, L. Yang, Z.H. Wang, H.S. Xia, Room-temperature self-healable and reprocessable polyurethane elastomers combined diels-alder bond and disulfide bond, Acta Polym. Sin. 50 (5) (2019) 527–534, https://doi.org/10.11777/j.issn1000-3304.2019.19021.
[17] H.H. Huang, W. Zhou, Z.Y. Zhong, S.S. Peng, X.H. Peng, Self-antiglare waterborne coating with superior mechanical robustness and highly efficient room-temperature self-healing capability, Prog. Org. Coating 146 (2020), https://doi.org/10.1016/j.porgcoat.2020.105717.
[18] J.R. Huang, Z. Gong, Y.K. Chen, A stretchable elastomer with recyclability and shape memory assisted self-healing capabilities based on dynamic disulfide bonds, Polymer 242 (2022), 124569, https://doi.org/10.1016/j.polymer.2022.124569.
[19] I. Magana, R. Lopez, F.J. Enriquez-Medrano, S. Kumar, A. Aguilar-Sanchez, R. Handa, R.D. de Leon, L. Valencia, Bioelastomers: current state of development, J. Mater. Chem. 10 (10) (2022) 5019–5043, https://doi.org/10.1039/d1ta09404a.
[20] Y.S. Gai, H. Li, Z. Li, Self-healing functional electronic devices, Small 17 (41) (2021), 2101383, https://doi.org/10.1002/smll.202101383.
[21] E. Malikmammadov, T.E. Tanir, A. Kiziltay, V. Hasirci, N. Hasirci, PCL and PCL-based materials in biomedical applications, J. Biomater. Sci. Polym. Ed. 29 (7–9) (2018) 863–893, https://doi.org/10.1080/09205063.2017.1394711.
[22] H. Kim, S.K. Ahn, D.M. Mackie, J. Kwon, S.H. Kim, C. Choi, Y.H. Moon, H.B. Lee, S. H. Ko, Shape morphing smart 3D actuator materials for micro soft robot, Mater. Today 41 (2020) 243–269, https://doi.org/10.1016/j.mattod.2020.06.005.
[23] D. Yan, Z.F. Wang, Z.J. Zhang, Stimuli-responsive crystalline smart materials: from rational design and fabrication to applications, Acc. Chem. Res. 55 (7) (2022) 1047–1058, https://doi.org/10.1021/acs.accounts.2c00027.
[24] Z.X. Deng, Y. Guo, X. Zhao, P.X. Ma, B.L. Guo, Multifunctional stimuli-responsive hydrogels with self-healing, high conductivity, and rapid recovery through host-guest interactions, Chem. Mater. 30 (5) (2018) 1729–1742, https://doi.org/10.1021/acs.chemmater.8b00008.
[25] Y.M. Ha, Y.O. Kim, Y.N. Kim, J. Kim, J.S. Lee, J.W. Cho, M. Endo, H. Muramatsu, Y. A. Kim, Y.C. Jung, Rapidly self-heating shape memory polyurethane nanocomposite with boron-doped single-walled carbon nanotubes using near-infrared laser, Compos. B Eng. 175 (2019), 107065, https://doi.org/10.1016/j.compositesb.2019.107065.
[26] G.D. Soto, C. Meiorin, D. Actis, P.M. Zelis, M.A. Mosiewicki, N.E. Marcovich, Nanocomposites with shape memory behavior based on a segmented polyurethane and magnetic nanostructures, Polym. Test. 65 (2018) 360–368, https://doi.org/10.1016/j.polymertesting.2017.12.012.
[27] Y.L. Xia, Y. He, F.H. Zhang, Y.J. Liu, J.S. Leng, A review of shape memory polymers and composites: mechanisms, materials, and applications, Adv. Mater. 33 (6) (2021), 2000713, https://doi.org/10.1002/adma.202000713.
[28] S. Xiao, J. Wei, S. Jin, X. Xia, L. Yuan, Q. Zou, Y. Zuo, J. Li*, Y. Li*, A multifunctional coating strategy for promotion of immunomodulatory and osteo/angio-genic activity, Adv. Funct. Mater. 33 (4) (2022), 2208968, https://doi.org/10.1002/adfm.202208968.
[29] B. Han, Y.L. Zhang, Q.D. Chen, H.B. Sun, Carbon-based photothermal actuators, Adv. Funct. Mater. 28 (40) (2018), 1802235, https://doi.org/10.1002/adfm.201802235.
[30] J.X. Shi, T.Z. Zheng, Y. Zhang, B.H. Guo, J. Xu, Cross-linked polyurethane with dynamic phenol-carbamate bonds: properties affected by the chemical structure of isocyanate, Polym. Chem. 12 (16) (2021) 2421–2432, https://doi.org/10.1039/d1py00157d.
[31] C.C. Chu, S.K. Yeh, S.P. Peng, T.W. Kang, W.J. Guo, J.T. Yang, Preparation of microporous thermoplastic polyurethane by low-temperature supercritical CO2 foaming, J. Cell. Plast. 53 (2) (2017) 135–150, https://doi.org/10.1177/0021955x16639034.
[32] T.Z. Liu, L.W. Liu, M. Yu, Q.F. Li, C.J. Zeng, X. Lan, Y.J. Liu, J.S. Leng, Integrative hinge based on shape memory polymer composites: material, design, properties and application, Compos. Struct. 206 (2018) 164–176, https://doi.org/10.1016/j.compstruct.2018.08.041.
[33] J. Zhang, C.Y. Shang, Z.E. Yu, L.X. Wang, J.K. Tang, F.R. Huang, Effect of the crosslinking degree on self-healing poly(1,2,3-triazolium) adhesive, Macromol. Rapid Commun. 43 (1) (2022), 2100236, https://doi.org/10.1002/marc.202100236.
[34] L.Z. Zhang, Z.H. Liu, X.L. Wu, Q.B. Guan, S. Chen, L.J. Sun, Y.F. Guo, S.L. Wang, J. C. Song, E.M. Jeffries, C.L. He, F.L. Qing, X.G. Bao, Z.W. You, A highly efficient self-healing elastomer with unprecedented mechanical properties, Adv. Mater. 31 (23) (2019), 1901402, https://doi.org/10.1002/adma.201901402.
[35] C.Q. Zhang, H.Y. Liang, D.S. Liang, Z.R. Lin, Q. Chen, P.J. Feng, Q.W. Wang, Renewable castor-oil-based waterborne polyurethane networks: simultaneously showing high strength, self-healing, processability and tunable multishape memory, Angew. Chem.-Int. Edit. 60 (8) (2021) 4289–4299, https://doi.org/10.1002/anie.202014299.
[36] Z.Q. Zhou, Y. Chen, A.H. Guo, T. Xue, X.W. Li, C.L. Yu, F.A. Zhang, Remotely fast response healing crosslinked polyurea nanocomposites with recyclability via two-step method, Compos. Sci. Technol. 224 (2022), 109462, https://doi.org/10.1016/j.compscitech.2022.109462.
[37] P.Y. Yan, W. Zhao, L. Jiang, B. Wu, K. Hu, Y. Yuan, J.X. Lei, Reconfiguration and shape memory triggered by heat and light of carbon nanotube-polyurethane vitrimer composites, J. Appl. Polym. Sci. 135 (5) (2018), 45784, https://doi.org/10.1002/app.45784.